Inorganic Chemistry

Article

pubs.acs.org/IC

Investigation of Counterion Influence on an Octahedral IrH_6-Complex in the Solid State Hydrides $AAeIrH_6$ (A = Na, K and Ae = Ca, Sr, Ba, and Eu) with a New Structure Type

K. Kadir,* D. Moser, M. Münzel, and D. Noréus

Department of Materials and Environmental Chemistry, Arrhenius Laboratory, Stockholm University, S-106 91 Stockholm, Sweden

Supporting Information

ABSTRACT: A number of new quaternary iridium based hydrides and deuterides $AAeIrH/D_6$ (where A = Na and K; Ae = Ca, Ba, Sr, and Eu) have been synthesized by direct combination of the alkali, alkaline earth or europium binary hydrides/deuterides and iridium powder. The crystal structures were determined by Guinier−Hägg X-ray and neutron powder diffraction and a new cubic structure type was found. The structure is described in *space group* $F\bar{4}3m$, but related to the K_2PtCl_6 type structure. The new structure can be described as consisting of cubes of A^+ and Ae^{2+} ions, where the A^+ and Ae^{2+} ions alternates so that they occupy opposite corners in the cube. Every second cube contains a regular octahedral $[Ir(III)H_6]^{-3}$-complex and the adjacent is empty. Solid-state IR spectroscopy was used to determine the Ir-allowed stretching and bending frequencies for the $[Ir(III)H_6]^{-3}$ complex with different counterions. These were also compared with the corresponding stretching frequencies for $Fe(II)H_6$, $Ru(II)H_6$, $Os(II)H_6$, and $Ir(II)H_5$ complexes in similar solid state hydrides, which increased when going from Fe through Ru, Os to Ir. The frequencies scaled almost linearly with the inverse of size of the cube surrounding the complexes but showed no significant dependence of the formal oxidation state or the experimentally obtained Ir−D distances. However, this was mainly because of difficulties in obtaining enough accurate atomic positions. The ab initio DFT calculations could reproduce the stretching frequencies within a few 10 cm^{-1}, indicating that experimental vibrational frequencies offer a sensitive test of DFT results.

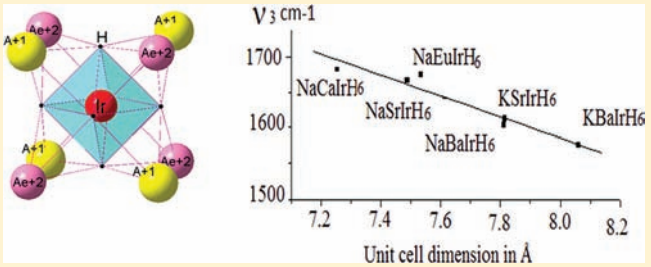

INTRODUCTION

Commercial hydrogen storage hydrides are typically interstitial hydrides, with hydrogen in the tetrahedral and octahedral sites of a more or less closed packed metal atom framework. As hydrogen enters the interstitial sites, the metal atom framework is only slightly adjusted to accommodate the hydrogen atoms. By selecting metals with different electropositivity and radii the stability of the metal hydride can be modified. The hydrogen storage capacity is, however, usually only one hydrogen atom per metal atom. In $LaNi_5$ based hydrides, used in rechargeable NiMH batteries, the storage capacity is just above 1 wt %.[1] In $TiMn_2$ based hydrides in the Daimler Benz pilot project (10 internal combustion engines vehicles) and in the submarine U212 project, the capacity barely reaches 2 wt %.[2]

If metal hydrides are synthesized from more electropositive and usually lighter alkali- and alkaline earth metals together with transition metals to the right of group V, there is a good chance that the transition metal will use the valence electrons from the alkali- and alkaline earth metals to form transition metal hydrido complexes. A large number of such hydrides have been synthesized. They are hydrogen rich, often with 2 or more hydrogen atoms per metal atom, but the strong and more covalent bond in the transition metal complexes makes them too stable for most applications. The metal atoms also undergo a significant rearrangement upon hydrogenation/dehydrogenation and several of the metal combinations do not even form a corresponding stable alloy; this precludes the modification of the properties by alloying. One of the first discovered hydrides of this type is the well investigated Mg_2NiH_4 system.[3]

However; the transition metal hydrido complexes of the first row have weaker transition metal hydrogen bonds and need a strong polarizing counterion, such as Mg^{2+} to be stabilized. Very few hydrides with a transition metal hydrido complex from the first row have been synthesized without having magnesium as counterion limiting the number of such hydrides found to date.[4] Nevertheless, this shows the importance of the counterion lattice for stabilizing transition metal hydrido complexes in the solid state, which is especially important for the lowest formal oxidation states on the central transition metal. Low oxidation states usually require good electron accepting ligands, where suitable ligand orbitals help to relieve the high electron density on the central atom (conventionally referred to as electron "back-donation"). In homoleptic complexes with hydrogen as ligand, this is not directly possible. In solid state hydrides, however, the easily deformable electron density of the very polarizable hydride ion H^- offers a mechanism to relieve the high electron density indirectly, by

Received: March 31, 2011
Published: October 28, 2011

Table 1. Observed and Calculated Data Including the ν_3 IR Stretching Frequencies for the Octahedral Complexes

compound	a calcd [Å]	a exp [Å]	x_H calcd	X_D exp	ω_3 calcd [cm^{-1}]	ω_3 exp [cm^{-1}]	ω_4 exp [cm^{-1}]	E_g [eV]	E_g[33] [eV]
$NaCaIrH_6$	7.23234	7.25448(9)	0.23187		1710	1684	852	3.33	
$NaCaIrD_6$		7.24543(3)		0.2302(5)		1222			
$NaSrIrH_6$	7.49929	7.48821(7)	0.22488		1678	1666	820	3.21	
$NaEuIrH_6$		7.53396(9)				1675			
$NaBaIrH_6$	7.8451	7.81083(3)	0.2151		1634	1603	776	3.09	
$NaBaIrD_6$		7.79852(9)		0.2148(3)		1152			
$KSrIrH_6$	7.80012	7.81264(4)	0.2168		1647	1612	813	3.01	
$KBaIrH_6$	8.08716	8.06016(6)	0.2094		1619	1575	730	2.91	
$KBaIrD_6$		8.04639(9)		0.2086(5)		1138			
Ca_2IrH_5		7.24757(8)				1689			
Sr_2IrH_5		7.61473(7)				1644			
Mg_2FeH_6	6.39850	6.430(1)	0.24358	0.2420					
Mg_2RuH_6	6.64668	6.6561	0.25364	0.251(2)	1753	1783		2.92	2.93
Ca_2RuH_6	7.2331	7.2269	0.23755		1570	1559		2.29	2.29
Sr_2RuH_6	7.62919	7.6088	0.22682		1482	1482		2.09	2.06
Ba_2RuH_6	8.09195	8.0283	0.21512	0.215(2)	1410	1438		1.69	
Mg_2OsH_6	6.69153	6.6828	0.25417		1825	1849		3.19	
Ca_2OsH_6	7.26471	7.253	0.23789		1656	1637		2.52	
Sr_2OsH_6	7.65585	7.6319	0.22687		1575	1575		2.28	2.26
Ba_2OsH_6	8.11763	8.046	0.21486	0.221(3)	1512	1505		1.81	

transferring it to the counterions in the solid state lattice.[5] In Mg_2NiH_4, close to tetrahedral $[NiH_4]$-complexes are counterbalanced by magnesium ions. The central nickel atom is in a formal zerovalent d^{10} oxidation state surrounded by four hydride ligands. Theoretical calculations of the electron structure show that the complex needs support from the small and strongly polarizing Mg^{2+} counterions for stability.[6,7] I.e the role of the counterions is to stabilize the complex by reducing the charge on the complex. In the related hydrides Li_2PdH_2 and Na_2PdH_2, this leads to metallic conductivity, when a small number of electrons are transferred to the alkali metal matrix from the linear 14 electron $[PdH_2]$-complex with formal zerovalent d^{10} palladium.[8] In a paper by Parker et al, where $A_2Pt(IV)H_6$ (A = alkali metal) compounds were studied, this effect was also shown to be important for higher formal oxidation states.[9] The high formal oxidation state of IV was reached by using a high hydrogen pressure in the kbar range in the synthesis to oxidize the central Pt-atom.

In this paper, this counterion influence upon the binding in the transition metal hydrido complexes is investigated in more detail. A thorough study of bonding trends requires a large numbers of hydrides and will therefore have to be carried out on hydrido complexes from the second or third row. We have focused our analysis on new hydrides based on Ir-complexes

A number of iridium based ternary hydrides with K_2PtCl_6 type structure have been synthesized, where a square pyramidal $[Ir(II)H_5]^{4-}$ complex is counterbalanced by divalent electropositive alkaline earth or rare earth metal ions in $Ca_2Ir(II)H_5$, $Sr_2Ir(II)H_5$, and $Eu_2Ir(II)H_5$,[10−12] or a higher oxidation number containing isolated $[Ir(III)H_6]^{-3}$ octahedra is counter balanced by either the alkali metal ions in $Li_3Ir(III)H_6$ and $Na_3Ir(III)H_6$ or by barium in $Ba_3Ir(III)_2H_{12}$.[13,14]

We describe a new series of quaternary iridium based hydrides $AAeIrH_6$ where isolated regular $[Ir(III)H_6]^{-3}$ octahedral complexes are counterbalanced by A^+ and Ae^{2+} cations. (A = Na and K; Ae = Ca, Ba, Sr, and Eu). IR vibration spectroscopy provided information of the transition metal hydrogen bond in the complexes, which were compared with earlier results from similar solid state hydrides. In a recent review, Parker pointed out that the most stringent test of a calculation is to compare the predicted and observed vibrational spectra. Indeed this is the best method to demonstrate that the calculation has converged to a genuine energy minimum rather than to a saddle point on the potential energy surface.[15]

EXPERIMENTAL SECTION

Syntheses. The starting alkali and alkaline earth metals ingots with 99% purity and Ir powder (99.9%) were all obtained from Aldrich. The binary hydrides/deuterides of alkaline earth metals were synthesized by direct combination of the elements. All handling of reactants and samples was done in a continuously purified argon glovebox to avoid oxidation.

The quaternary compounds were prepared by sintering (∼2 g) pressed tablets that had been compacted in a tablet press at about 3 kbar from powder mixtures of the binary hydrides/deuterides of alkaline−alkaline earth metals and iridium powder in the atomic ratio $AAeIrH_6/D_6$ = 1:1:1. The tablets were sintered in a tube furnace at 400 °C (in 5 MPa hydrogen/deuterium gas). After they were cooled, the samples were crushed and a small sample was removed for X-ray analysis of the reacted phases. New tablets were repressed and reheated as described above, but the temperature was raised stepwise from 400 to 510 °C. At each temperature setting, the samples were held for 3 h. Several attempts were made before the optimum synthesis conditions could be found.

X-ray diffraction photographs were obtained from a subtraction-geometry Guinier−Hägg focusing camera, using strictly monochromated Cu Kα_1 radiation.[16] A single-coated X-ray film (CEA Reflex 15) was used throughout the work. The films were evaluated by means of a computer-controlled single-beam microdensitometer designed for the scanning analysis of X-ray powder photographs.[17] The θ scale was calibrated with an internal (silicon) standard, using a parabolic correction curve. To locate the hydrogen atoms in the new hydrides, the deuterides $NaCaIrD_6$, $NaBaIrD_6$ and $KBaIrD_6$ were prepared for neutron diffraction. The diffraction patterns were recorded at the R2 reactor in Studsvik using a cylindrical vanadium sample holder (Ø = 5 mm) and a neutron wavelength of 1.47 Å at 295 K.

IR Spectroscopy. The IR-measurements were done in air with a Bruker IFS-55 spectrometer with a resolution of 2 cm^{-1}, typically in the 350−5000 cm^{-1} range at ambient temperature. One hundred scans were carried out per sample. The sample was mixed with Nujol and fixed between KBr-windows and the data was collected by OPUS 5.0

dx.doi.org/10.1021/ic200662m | Inorg. Chem. 2011, 50, 11890−11895

software. All spectra have been normalized to absorption of 1 at 5000 cm^{-1}.

Calculations. The density functional theory (DFT) calculations (electronic structure and vibrational modes at Gamma point) were performed using the generalized gradient approximation (GGA) with the PW91 gradient dependent functional implemented in the VASP code.[18−20] PAW pseudopotentials were used to describe the electron wave functions.[21] For Sr and Ba semicore s electrons, for Mg semicore p electrons were also included in the calculation.

An energy cutoff of 500 eV was used for all the calculations and k-points sampling was performed on a 4 × 4 × 4 Monkhorst-Pack grid with a shift of 0.125 to include the Γ point.[22] Necessary convergence tests were fulfilled and total energies were converged to at least 1 meV/f.u. All structures were fully relaxed with forces converging to less than 0.001 eV $Å^{-1}$.

The optimization of the internal coordination is a crucial task in order to have zero-pressure and zero-forces for correct calculations of vibrations. The equilibrium parameters V_{eq}, E_0, B, B' were therefore obtained by fitting E versus V values to a Birch−Murnaghan equation of state. This is done by steps optimizing the ionic positions for every fixed volume.

In the initial structural input atoms were positioned as suggested from experimental data of $NaCaIrD_6$.

Theoretical equilibrium parameters are collected in Table 1 together with the experimental data. The experimental hydrogen positions are assumed to be the same as those refined from the deuterated analogues.

The vibrational modes at Γ point were calculated using Finite Differences as implemented in VASP. Each atom is displaced, one at a time, by a small distance along each of the Cartesian directions and the force acting on each atom inside the cell was determined. The displacement has to be small in order to remain in the range of harmonic approximation. Here we used a value of 0.02 Å.

The force constant matrix is determined by dividing the force by the displacement. The diagonalization of the dynamical matrix yields the eigenvalues (frequencies) and eigenvectors.

Only zone-centered (Γ-Point) frequencies are requested in order to compare with the normal modes frequencies from Raman and IR experiments, which only couple to near $q = 0$ modes. To get the lattice vibrational dispersion relations the calculation would require the diagonalization of the wave-vector-dependent ($D(q)$) dynamical matrix with $\mathbf{q}$ within the first Brillouin zone.

Symmetry dramatically reduces the number of the necessary displacements and this is exploited in this paper. To determine whether the normal modes are internal (octahedral 6H and 1 Tm) or if the dispersion inside the lattice has an important effect, calculations were performed by displacing either all the atoms or just those in the octahedra, and the obtained frequencies compared. No difference was found between the zone center normal modes ν_1(Raman active) and ν_3 (IR active) obtained with the two methods. This allowed us to focus only on the octahedral system saving computational time. This assumption ceases to be valid for lower frequencies normal modes where the A/Ae atom contributes to the lattice vibrations (external modes).

RESULTS AND DISCUSSION

Crystal Structure. Using the TREOR program[23] and the least-squares refinements program PIRUM,[24] the X-ray powder pattern of $ABIrH_6/D_6$ (where A = Na and K; Ae = Ca, Ba, Sr, and Eu) could be indexed on the basis of a cubic face centered structure with unit cell dimensions increasing with the A and Ae metal radius.

The positions of the metal atoms were found by direct methods using SHELXS to form an AlLiSi type structure, described in the space group $F\bar{4}3m$ (216).[25,26]

Rietveld refinements based on X-ray and neutron powder patterns of $AAeIrH_6/D_6$ showed the total structure to be of a new structure type where an IrD_6-complex substitutes the Al atom in the AlLiSi type structure. Crystallographic parameters and Rietveld R-values are given in Table 2. Ir atoms are in position 4*a*, A atoms in 4*d*. Ae atoms occupy the 4*c* sites and hydrogen or deuterium 24*f* (x 0 0) position ($x \approx 0.2$). By analyzing the X-ray diffraction patterns, the metal atomic positions of $KSrIrH_6$, $NaSrIrH_6$ and $NaEuIrH_6$ were found to be isomorphous to those in $KBaIrH_6/D_6$, $NaCaIrH_6/D_6$ and $NaBaIrH_6/D_6$. No corresponding deuterides were prepared. The XRD data is included in the Supporting Information.

Table 2. Crystallographic Parameters and Interatomic Distances in (Å) for ($AAeIrH_6/D_6$ Where A= Na and K, Ae = Ca, Sr, Ba and Eu) in Space Group $F\bar{4}3m$ (216) and Z = 4[a]

atoms	site	atom position x	y	z	occupancy
Ir	4*a*	0.000	0.000	0.000	1
A (Na, K)	4*d*	0.750	0.750	0.750	1
Ae (Ca, Sr, Ba and Eu)	4*c*	0.250	0.250	0.250	1
A (Na, K)	4*d*	0.750	0.750	0.750	1
D	24*f*	x	0.000	0.000	1

		$NaCaIrD_6$	$NaBaIrD_6$	$KBaIrD_6$
R_P (%)		3.39	4.89	5.29
R_{wp} (%)		6.60	6.46	7.57
R_F (%)		2.08	4.01	5.18
x		0.2302(5)	0.2148(3)	0.2086(5)
B_{iso} A ($Å^2$)		1.4(3)	2.8(2)	1.2(2)
B_{iso} Ae ($Å^2$)		3.7(3)	0.4(1)	0.6(2)
B_{iso} Ir ($Å^2$)		0.5(4)	0.6(1)	1.3(1)
B_{iso} D ($Å^2$)		1.48(1)	2.2(1)	3.4(1)
Ir−D	× 6	1.6713(6)	1.674(4)	1.6797(5)
(A,Ae) D	× 12	2.5643(4)	2.7707(5)	2.8892(6)
(A,Ae)−Ir	× 6	3.1360(3)	3.3766(4)	3.5128(3)
D−D	× 4	2.364(6)	2.367(5)	3.3604(6)

[a]The structure was refined by using the Rietveld refinement program RIET and FULLPROF[36] for $NaCaIrD_6$. SHELXL97[25] was used for interatomic distances.

The new $AAeIrH_6$ structure in Figure 1 can be viewed as a *ccp* array of $[Ir(III)H_6]^{3-}$ octahedra with A^+ and Ae^{2+} ions alternatingly filling the interstitial tetrahedral sites. The structure can also be described as consisting of A^+ and Ae^{2+} ion cubes, with the alkali A^+ and Ae^{2+} ions alternating so that they occupy opposite corners in the cube, and where every second cube contains an $[Ir(III)H_6]^{3-}$ complex and the adjacent is empty. This way of arranging the counterions has also been found in the $MgCaNiH_4$ and $MgEuNiH_4$ hydrides but in these cases the "cube" around the complex is distorted.[27]

The related K_2PtCl_6 type structure, with only one kind of counterion and complex, forms an antifluorite structure and is a common structure for many quaternary hydrides of this type, including the series Ae_2TmH_6 (Ae = Mg, Ca, Sr, Ba and Tm = Fe, Ru Os). In the DFT calculations, this family is compared to the new Ir systems presented in this paper. As it will be discussed below, Ba_2FeH_6 has not yet been successfully synthesized and Ca_2FeH_6 and Sr_2FeH_6 only with difficulty in reactions with low yields.[28]

The DFT calculations were in good agreement with the observed unit cell parameters and refined hydrogen positions when available, as listed in Table 1.

The colors of $NaCaIrH_6$ (rose), $NaBaIrH_6$, $KBaIrH_6$ (light-yellow), $KSrIrH_6$ (light brown), $NaSrIrH_6$ (white), and

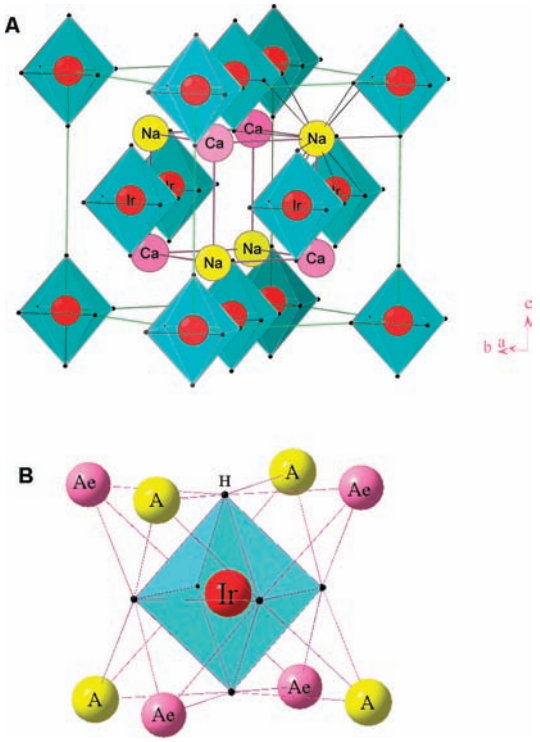

Figure 1. (a) Array of $[Ir[III]H_6]^{3-}$ in the octahedral sites of $NaCaIrH_6$ stabilized by Na^+ and Ca^{2+}. DIAMOND[35]. (b) Structural unit of $AAeIrH_6$, showing the capping of the octahedra $[Ir[III]H_6]^{3-}$ by A^+ and Ae^{2+}.

$NaEuIrH_6$ (yellow) indicate that these hydrides are insulators with a significant band gap in agreement with calculated values in Table 1. Attempts were also made to include the corresponding hydrides with Mg as counterion, but efforts yielded hydrides with different structure types and will be the subject of another paper. We resynthesised Ca_2IrH_5 and Sr_2IrH_5 to remeasure unit cell dimensions and Ir frequencies. Ca_2IrH_5 was found to be brown and Sr_2IrH_5 (white), while Moyer described both compounds as black.[10]

Evaluation of IR Spectroscopy. In a perfect octahedron, there is one IR-active stretching mode ν_3 and one bending mode ν_4.[29] In our data the stretching mode ν_3 dominated the spectra but was split in closely lying peaks giving it an irregular shape as seen in Figure 2, and in the spectra supplied in the Supporting Information for the other hydrides. The irregular shape has previously been found by Preetz et al in studies on the related hydrides A_2PtH_6 (A = Na, K and Rb).[30] They found three closely lying peaks with increasing intensity for increasing wave numbers. This is probably also the reason behind the observation of an unusually broad ν_3 peak with a significant asymmetry also observed in earlier studies on other octahedral hydrido complexes.[5] From studies on a PtH_6^{2-} complex, Parker et al. suggested it to come from Fermi resonance effects.[9] This seems to be a general problem for these types of octahedral hydrido complexes, where the three bending modes cluster close together at about half the frequency of the stretching modes which are also not so far separated from each other. As we only have IR data available from the samples, we do not want to make a deeper analysis of the spectra but limit ourselves to observe the general trends of the ν_3 peaks. To estimate the maximum position of the ν_3 peaks, these were fitted by a Gaussian function. This also minimizes the influence

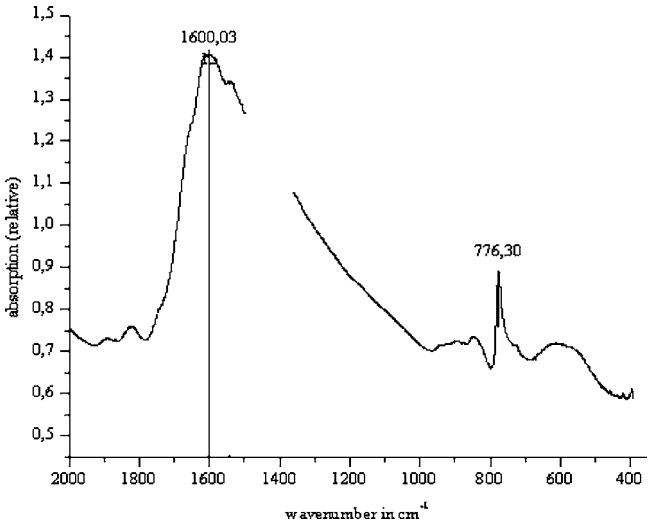

Figure 2. Spectrum of $NaBaIrH_6$ in the range of 2000 cm^{-1} to 350 cm^{-1}. The area with the Nujol background peaks between 1495 cm^{-1} and 1360 cm^{-1} has been removed for clarity.

from superposed water bending-vibration coming from moisture in the air. Figure 2 shows the $NaBaIrH_6$ spectrum with the ν_3 (peak 1600 cm^{-1}, Gaussian fit 1602.6 cm^{-1}) and ν_4 (peak 776.3 cm^{-1}). The area with the Nujol background peaks between 1495 cm^{-1} and 1360 cm^{-1} has been removed for clarity. The small peak above the ν_3 frequency has also been observed in Ae_2RuH_6 complexes (Ae = Ca, Sr, and Eu) and could probably be a combinatorial peak as suggested by Moyer et al.[31,32] By comparing with the calculated frequencies given in Table 3, it can also be traces from the IR-forbidden stretching frequencies becoming visible by lattice effects. The ratio between the hydride and deuteride samples of the same metal composition is 1.41 for $NaBaIrH/D_6$ as is expected because of the isotopic mass substitution. The values of $NaCaIrH/D_6$ (1.38) and $KBaIrH/D_6$ (1.37) are slightly lower. The ratio of the maximum of ν_3 and ν_4 is roughly 2:1 for all the hydrides.

CONCLUSIONS AND COMPARISON WITH OLDER DATA

The unit cell dimension for all these hydrides based on Fe, Ru, Os, and Ir complexes correlates linearly with the sum of the Pauling counterion radius, as shown in Figure 3. Interestingly the magnesium containing hydrides form a small group separated from the rest.

Figure 4 shows the frequencies of the ν_3 (M−H) vibration plotted against the inverse of the cubic unit cell dimension. The frequency increases when going from Fe through Ru and Os to Ir indicating a general increase in transition metal hydrogen bond strength.

The additional influence on the frequencies from the different counterion surroundings shows a fairly linear dependence of inverse of the cubic unit cell axis except for the magnesium containing hydrides. The strong correlation between counterion sizes and vibrational frequencies indicate that the electropositivity of the counterion is of secondary importance, however it should not be neglected. The large H^- ion would be very sensitive to the space correlation of any charged counterion surrounding the complex. The calculated results from the Fe, Ru, and Os complexes compare well with

dx.doi.org/10.1021/ic200662m | Inorg. Chem. 2011, 50, 11890–11895

Table 3. Calculated Vibrational Frequencies for $AAeIrH_6$ (A= Na and K, Ae = Ca, Sr, and Ba)

$NaCaIrH_6$	$NaSrIrH_6$	$NaBaIrH_6$	$KSrIrH_6$	$KBaIrH_6$				
2030	2024	2004	2002	1989	A1g	1	Raman	stretching
2020	2010	1990	1987	1975	Eg	2	Raman	stretching
1710	1678	1634	1647	1619	T1u	3	IR	strecthing
882	898	898	859	850	T1u	4	Raman	bending
825	830	827	813	803	T2g	5	IR	bending
795	760	723	788	769	T2u	6	inactive	bending
410	405	375	441	431	T1g	7	inactive	librations
95	98	83	89	84	T2g	8	Raman	translations

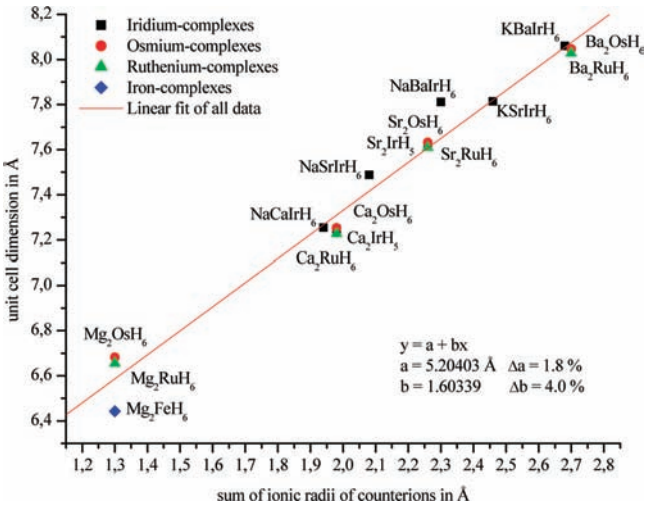

Figure 3. Dependence of unit cell dimension on the ionic radii of the counterions.

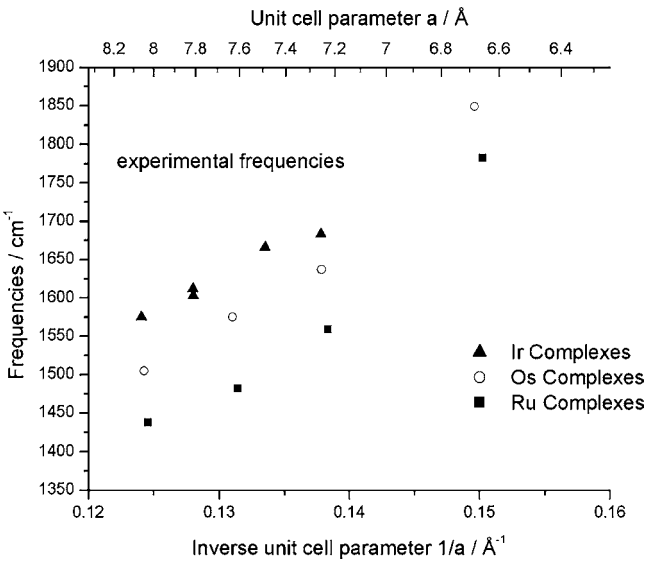

Figure 4. Experimental Ir active stretching frequencies show a close to linear dependence of the inverse cubic unit cell parameter when Mg is not part of the counterion lattice.

earlier published results.[33] This shows that vibrational frequencies are a very sensitive test for DFT calculations and thus also for a better understanding of the electronic structure. Because of the difficulties in obtaining enough accurate Ir−D distances, these are not so good in this respect. The large bandgaps of about 3 eV would point to a white to yellow−white color of the compounds, which is also observed for several of them. Deviations are probably due to impurities from the synthesis or local nonstoichiometries.

Again Mg stands out for having positive effects in compressing and helping to stabilize these hydrido complexes. These results with magnesium counterions are interesting, as is manifested in the details of the calculations. Generally the transition metal p electrons take part in the bonding only to a lesser extent. This is in agreement with suggestions by Firman and Landis and confirmed in our previous work on Ni- and Pd-hydrido complexes, leaving mainly the d- and s-electrons responsible for the bonding in the complex.[7,8,34] Furthermore, there is a low contribution from the first row transition metal d-states to this bonding, making the complexes from the first row significantly weaker than those from the second and third row transition metals. This is simply to say that 4d and 5d orbitals are more diffuse and better suitable for bonding with the soft hydrogen ligands than 3d orbitals. In the hydrides not having Mg as counterions, the complexes behave more molecular-like and the bands in the eDOS can be directly identified by their molecular counterparts. This can be seen in Figure 5 where the eDOS of Mg_2OsH_6 and Ba_2OsH_6 are compared.

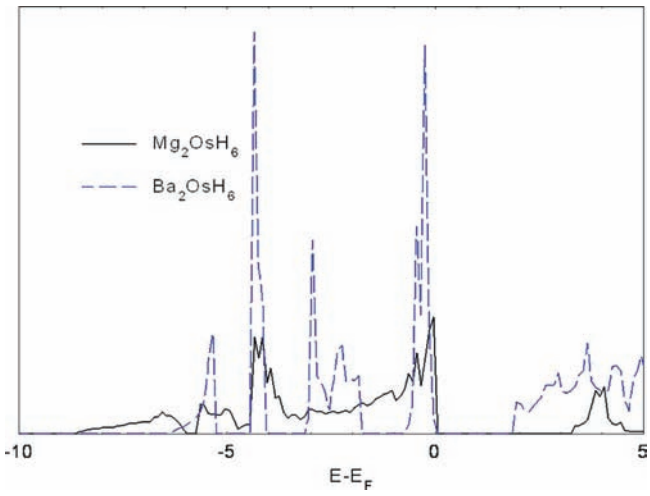

Figure 5. eDOS of Mg_2OsH_6 and Ba_2OsH_6. In Ba_2OsH_6, the complexes behave more molecular-like and the bands can be identified with their molecular counterparts. In Mg_2OsH_6, the situation is more similar to an interstitial hydride where the bond between hydrogen and the metals are on a more similar footing.

If magnesium is not part of the counterion framework, we obtain a fairly simple picture of the complexes, with rather independent molecular-like complexes suspended in cation framework, where the vibrational frequencies scale rather linearly with the space available depending on the radii of the counterions.

dx.doi.org/10.1021/ic200662m | Inorg. Chem. 2011, 50, 11890–11895

With Mg as counterion the situation is more complex. The eDOS presents mixed regions with complex bands overlapping each other, as the hydrides become partly ionic ($Mg^{2+}(H^-)_2$) and partly hydrido complexes. Two main features are identified: (a) the requirement of the polarizing Mg^{2+} for a small H coordination number acts as an internal pressure and compresses the complexes and (b) the ionic contribution helps to keep the hydrides together. These add up to a stronger bonding mechanism which is probably the reason why we could not obtain any corresponding Mg containing hydride of the new structural type presented in this paper but only hydrides with different structures.

This can also explain why almost no hydrido complex based on the first row transition metal have been found without including Mg in the counterion framework as this stronger bonding mechanism is needed to support the first row transition metal hydrido complexes. This understanding may, however, offer an opportunity to find more practical hydrogen storage systems.

The stability of hydrides based on complexes from the second and third row transition metals can not be much modified as the transition metal−hydrogen bonding is strong and only marginally influenced by the counterion framework. These hydrides are anyhow too heavy and the metals too expensive for practical applications. More hope lies within the first row transition metals, the hydrogen bonds of which are weaker and need a polarizing Mg to keep the structure together. On one hand, the presence of Mg introduces changes in the internal environment of metal hydrido complexes toward interstitial-like hydrides that can be more easily modified by the counterions. On the other hand, too much Mg as in Mg_2FeH_6 and Mg_2NiH_4 makes the compounds too stable but those could be destabilized by trying to substitute some of the Mg with a less polarizing counterion. A problem for applications is, however, to prevent the less stable hydrides from forming the more stable magnesium-rich variants during practical hydrogen cycling.

■ ASSOCIATED CONTENT

Ⓢ Supporting Information

Observed and calculated, $1/d^2$-values and intensities for AAeIrH/D_6 from Guinier−Hägg X-ray diffraction data using Cu Kα_1 radiation and Si as the internal standard at 293 K, the corresponding diffraction spectra from $NaCaIrH_6$, $NaSrIrH_6$, and $NaEuIrH_6$, as well as the difference plots obtained in the profile refinement of the NPD for $NaCaIrD_6$, $NaBaIrD_6$, and $KBaIrD_6$, and IR-spectra of all $NaCaIrH_6$, $KBaIrH_6$, $NaSrIrH_6$, $KSrIrH_6$, and $NaEuIrH_6$. This material is available free of charge via the Internet at http://pubs.acs.org.

■ AUTHOR INFORMATION

Corresponding Author

*E-mail: karim@mmk.su.se. Tel: (46) 8 16 23 83. Fax: (46) 8 16 31 18.

■ ACKNOWLEDGMENTS

We are grateful to Håkan Rundlöf for collecting the neutron diffraction pattern at R2 reactor in Studsvik and Dr. Lars Eriksson for helpful discussions and supplying us with Grusplot and Pfilm programs. This work has been supported by the European Commission DG Research (contract SES6-2006-518271/NESSHY) and the Swedish Energy Agency.

■ REFERENCES

(1) WillemsJ. J. G.Philips J. Res.1984
(2) Bernauer, O.; Toepler, J.; Noréus, D.; Hempelmann, R.; Richter, D. *Int. J. Hydrogen Energy* **1989**, *14*, 187−200.
(3) Reilly, J. J.; Wiswall, R. H. Jr. *Inorg. Chem.* **1968**, *7*, 2254.
(4) Kadir, K.; Noréus, D. *Inorg. Chem.* **2007**, *46*, 2220; *Inorg. Chem.* **2009**, *48*, 3288.
(5) Kritikos, M.; Noréus, D. *J. Solid State Chem.* **1991**, *93*, 256.
(6) Miller, G. J.; Deng, H.; Hoffmann, R. *Inorg. Chem.* **1994**, *33*, 1330.
(7) Häussermann, U.; Blomqvist, H.; Noréus, D. *Inorg. Chem.* **2002**, *41*, 3684.
(8) Olofsson-Mårtensson, M.; Häussermann, U; Tomkinson, J; Noréus, D. *J. Am. Chem. Soc.* **2000**, *122*, 6960.
(9) Parker, S. F.; Bennington, S. M.; Ramirez-Cuesta, A. J.; Auffermann, G.; Bronger, W.; Herman, H.; Williams, K. P. J.; Smith, T. *J. Am. Chem. Soc.* **2003**, *125*, 11656.
(10) Moyer, R. O. Jr.; Stanitski, C.; Tanaka, J.; Kay, M. I.; Kleinberg, R. *J. Solid State Chem.* **1971**, *3*, 541.
(11) Bronger, W. *Angew. Chem.* **1991**, *103*, 776−784; *Angew. Chem., Int. Ed. Engl.* **1991**, *30*, 759.
(12) Bronger, W.; Jansen, K.; Breil, L. *Z. Anorg. Allg. Chem.* **1998**, *624*, 1477.
(13) Bronger, W.; Gehlen, M.; Auffermann, G. *J. Alloys Compd.* **1991**, *176*, 255.
(14) Kadir, K.; Noréus, D. *J. Alloys Compd.* **1994**, *209*, 213.
(15) Parker, S. F. *Coord. Chem. Rev.* **2010**, *254*, 215.
(16) Johansson, T. *Naturwissenschaften.* **1932**, *20*, 758; *Z. Phys.* **1933**, *82*, 507.
(17) Johansson, K. E.; Palm, T.; Werner, P.-E. *J. Phys. (Paris)* **1980**, *E13*, 1289.
(18) Perdew, J. P.; Yue, W *Phys. Rev. B* **1986**, *33* (12), 8800−8802.
(19) Perdew, J. P.; Wang, Y *Phys. Rev. B* **1992**, *45* (23), 13244−13249.
(20) Kresse, G; Hafner, J. *Phys. Rev. B* **1993**, *47* (1), 558−561. Kresse, G; Furthmuller, H *Phys. Rev. B* **1996**, *54* (16), 11169−11186.
(21) Blochl, P. *Phys. Rev. B* **1994**, *50* (24), 17953−17979.
(22) Monkhorst, H; Pack, J *Phys. Rev. B* **1976**, *13* (12), 5188−5192.
(23) Werner, P.-E.; Eriksson, L.; Westdahl, M. *J. Appl. Crystallogr.* **1985**, *18*, 367.
(24) Werner, P.-E.; Eriksson, L. *World Directory of Powder Diffraction Programs*, release 2.12; International Union of Crystallography: Chester, 1993.
(25) Sheldrick, G. M. *Acta Crystallogr.* **1990**, *A46*, 467.
(26) Nowotny, H.; Holub, F. *Monatsh. Chem.* **1960**, *91*, 877.
(27) F. Gingl, F; Yvon, K. *Z. Kristallogr.* **1993**, *207*, 247.
(28) Huang, B.; Bonhomme, F.; Selvam, P.; Yvon, K. *J. Less-Common Met.* **1991**, *179*, 301.
(29) Nakamoto, K.; *Infrared and Raman Spectra of Inorganic and Coordination Compounds*; Wiley: New York, 1978; pp 151.
(30) Bublitz, D.; Peters, G.; Preetz, W.; Auffermann, G.; Bronger, W. *Z. Anorg. Allg. Chem.* **1997**, *623*, 184.
(31) Moyer, R.O. J.R.; Wilkins, J. R.; Ryan, P. *J. Alloys Compd.* **1999**, *290*, 103.
(32) Hagemann, H.; Moyer, R. O. *J. Alloys Compd.* **2002**, *330−332*, 296.
(33) Halilov, S. V.; Singh, D. J.; Gupta, M.; Gupta, R. *Phys Rev. B.* **2004**, *70*, 195117.
(34) Firman, T. K.; Landis, C. L. *J. Am. Chem. Soc.* **1998**, *120*, 12650−1265.
(35) Bergerhoff, G. *DIAMOND—Visual Crystal Structure Information System*; Gerhard-Domagk-straBe. 1, 53121: Bonn, Germany, 1996.
(36) Rodriguez-Carvajal, J. *FULLPROF.2k*, version *3.00 - Nov2004-LLB JRC*; Gifsur-Yvette: Cedex, France, 2004.